International Journal of Nanomedicine

Dovepress
Taylor & Francis Group

Open Access Full Text Article

ORIGINAL RESEARCH

Nano-Biomimetic Fibronectin/Lysostaphin-Co-Loaded Silk Fibroin Dressing Accelerates Full-Thickness Wound Healing via ECM-Mimicking Microarchitecture and Dual-Function Modulation

Chen-Ting Liu[1], Li-Dan Huang[2], Kai Liu[3], Ke-Fan Pang[1], Hao Tang[3], Ting Li[3], Yang-Pei Huang[4], Wei-Qin Zhang[1], Jun-Juan Wang[3], Guo-Li Yin[3], Kou-Zhen Hua[3]

[1]School of Clinical Medicine, Hangzhou Medical College, Hangzhou, Zhejiang, 310053, People's Republic of China; [2]Laboratory Medicine, Yiwu Blood Station, Yiwu, Zhejiang, 322000, People's Republic of China; [3]School of Basic Medical Sciences and Forensic Medicine, Hangzhou Medical College, Hangzhou, Zhejiang, 310053, People's Republic of China; [4]School of Laboratory Medicine, Hangzhou Medical College, Hangzhou, Zhejiang, 310053, People's Republic of China

Correspondence: Kou-Zhen Hua; Guo-Li Yin, School of Basic Medical Sciences and Forensic Medicine, Hangzhou Medical College, Hangzhou, People's Republic of China, Email 2006031055@hmc.edu.cn; 22007882@qq.com

Purpose: In cases of large-area skin defects, the absence of extracellular matrix can lead to difficulties in fibroblast migration, thereby hindering wound healing. This study aimed to address the challenges in treating skin defects by developing a biomimetic nano-dressing that both has antibacterial properties and promotes healing by mimicking the extracellular matrix.

Patients and Methods: The electrospun silk protein nanofibers were ultrasonically fragmented into staple fibers. These were then coated and modified by adding a collagen (Col) solution loaded with recombinant lysostaphin (rLys) and fibronectin (Fn), ultimately constructing a biomimetic nanosponge (Fn-rLys-Col/SF-S).

Results: In vitro studies have shown that Fn-rLys-Col/SF-S possesses good water vapor balance and antibacterial properties, is non-toxic to cells, and can promote cell proliferation and migration. In vivo experimental results indicated that Fn-rLys-Col/SF-S healed a week earlier than the control group, with the structure of the newly formed skin resembling normal skin at 21 days. Further immunohistochemistry and qRT-PCR results demonstrated that Fn-rLys-Col/SF-S effectively promotes the healing of skin defect wounds by reducing inflammation, promoting angiogenesis, enhancing collagen deposition, and regulating the degree of fibrosis.

Conclusion: In conclusion, the Fn-rLys-Col/SF-S biomimetic sponge dressing can promote the repair of skin defects by mimicking the extracellular matrix, providing a potential therapeutic strategy for clinical wound treatment.

Keywords: electrospinning, silk fibroin, fibronectin, recombinant lysostaphin, wound healing

Introduction

The skin, the largest and most injury-prone organ in the human body, serves as the first line of defense, protecting internal tissues and organs while maintaining internal environmental stability.[1] Once the skin is damaged, it undergoes a repair process consisting of four stages: hemostasis, inflammation, proliferation, and tissue remodeling.[2] Small wounds can heal on their own, but clinical intervention is often needed when the diameter of a skin defect exceeds 2 cm. The difficulty in repairing large skin defects is mainly because the basal layer at the defect site lacks epithelial cells, and the epithelial cells on both sides lack extracellular matrix(ECM) for migration and attachment, making it difficult for cells to effectively cover the wound, leading to challenges in closing the wound.[3,4] Furthermore, prolonged wound exposure can lead to bacterial infection,[5] excessive inflammation,[6] and insufficient angiogenesis,[7] further hindering the healing process and resulting in chronic wounds that are difficult to heal, imposing physiological, psychological, and economic burdens on patients.[8,9]

Received: 28 February 2025
Accepted: 27 May 2025
Published: 12 June 2025

Graphical Abstract

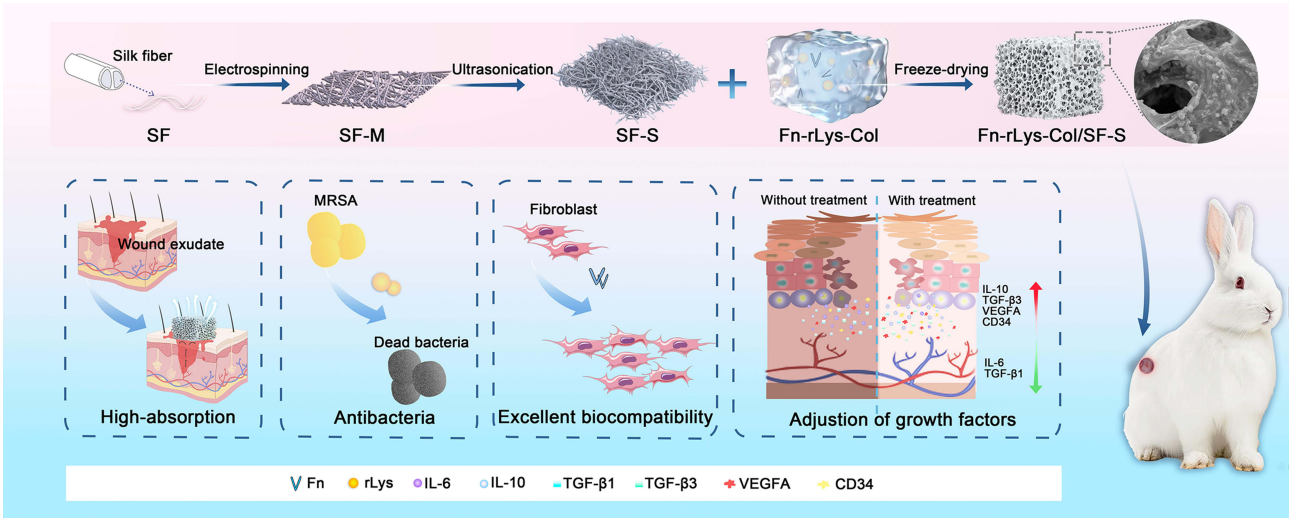

Dressings are fundamental tools for wound management. Modern dressings mainly include membranes,[10] foams,[11] and hydrogels.[12] Besides traditional functions of isolation and exudate absorption, they maintain wound humidity; especially non-adherent hydrogels have been clinically promoted. However, existing functional dressings generally have low porosity,[13] poorly biomimetic microstructure,[14] insufficient cell infiltration, and vascularization, with inadequate transport of nutrients, oxygen, and metabolic products.[15] This presents challenges in treating large skin defects or chronic non-healing wounds. Electrospinning technology can prepare nanofiber membranes that have a large surface area and high porosity, with nanostructures that can mimic extracellular matrices,[16] and are widely used in tendons,[17] cartilage,[18] and skin.[19] However, previous research indicates that nanomembranes prepared solely by electrospinning are two-dimensional structures with small pore sizes, unfavorable for three-dimensional cell growth. The development of materials with large pore sizes and nanobionic ECM characteristics is the direction for developing biomimetic dressings. Therefore, the innovation of this study lies in using electrospinning technology combined with ultrasonic fragmentation and freeze-drying techniques to prepare a dressing matrix with a large pore, three-dimensional bionic structure to improve water vapor exchange, antibacterial properties, and cell regulation functions, and to achieve the loading and sustained release of active drugs.

The three-dimensional microstructure of dressings can regulate tissue cell growth. Introducing cytokines can significantly improve the biological function of dressings, acting as carriers for the local release of cytokines, synergistically promoting tissue repair with the dressings.[20] Silk fibroin (SF) is widely recognized for its spinnability, biocompatibility, and biodegradability,[21,22] making it an ideal wound dressing matrix material. Numerous studies have shown that silk fibroin and collagen composite dressings have good biocompatibility and mechanical properties.[23–25] However, the system of pure silk fibroin and collagen has limited capabilities in regulating cell behavior and antimicrobial activity. Therefore, another innovation of this study is utilizing the high viscosity of collagen to encapsulate and carry active agents like fibronectin and lysozyme. Fibronectin (Fn) is a large glycoprotein in the ECM, promoting cell-ECM adhesion through α5 β1 integrin, regulating cell adhesion, migration, proliferation, and differentiation, and participating in the wound healing process, conferring multiple biological activities.[26] However, its application in wound repair-related research is limited. Lysozyme is a naturally occurring glycoside hydrolase that hydrolyzes the peptidoglycan layer of Gram-positive bacteria cell walls, playing a critical role in protecting wounds from bacterial, especially antibiotic-resistant bacterial infections.[27] Also, due to its safety, it is called a "green antibiotic".[28]

In this study, SF, with high biocompatibility and biomechanics, is used as the base material. Nanometer short fibers of silk fibroin (SF-S) are prepared using electrospinning and ultrasonic fragmentation as the bionic extracellular matrix

scaffold. The collagen gel loaded with Fn and rLys active proteins is combined with SF-S and constructed into a biomimetic multifunctional dressing (Fn-rLys-Col/SF-S) with a large-pore structure by freeze-drying. The structure and in vitro biological properties are systematically analyzed and tested in a full-thickness skin defect model on rabbits' backs, using HAINUO sterile medical dressings (abbreviated as SHISHOU) as controls to evaluate its potential as a wound dressing.

Material and Methods

Materials and Equipment

Materials

Col was obtained from FUSHENBIO (Shanghai, China). rLys was synthesized by our group. Fn was obtained from UKFORBERUN INTERNATIONAL (Henan, China). ATCC (Manassas, VA, USA) supplied human foreskin fibroblast (HFF), *Escherichia coli* (*E. coli*, ATCC 252922), *Pseudomonas aeruginosa* (*P. aeruginosa*, ATCC 15442), *Staphylococcus aureus* (*S. aureus*, ATCC 25923), and *Methicillin-resistant Staphylococcus aureus* (MRSA, ATCC 43300). The rabbit operation table (NJR-20) was supplied by Techman Software Co., Ltd. (Chengdu, China). Phosphate buffered saline (PBS), DMEM, cell counting kit-8 (CCK-8), fetal bovine serum (FBS), paraformaldehyde, Calcein AM Cell Viability Assay Kit (CCK-F) were obtained from Beyotime (Shanghai, China). The sheep whole blood was purchased from Yuhuan Southern Reagent Co., Ltd. (Zhejiang, China).

Equipment

Electrospinning machine (E02-001) was obtained from Foshan Nanofiberlabs Co., Ltd. (Guangdong, China). Ultrasonic cell disruptor (JY92-IIN) was obtained from Scientz (Ningbo, China). Lyophilizer (MODULYOD-230) was obtained from Thermo Fisher Scientific (USA). Scanning Electron Microscope (SEM, Quanta 200) was sourced from FEI NanoPorts (Shanghai, China).

Preparation of Dressing

Synthesis of Silk Fibroin Short Fibers

A 20% silk fibroin formic acid solution is electrospun into silk fibroin nanomembranes (SF-M) under the parameters of a voltage of 17.6 kV, a feed rate of 4.0 mL/h, and a receiving distance of 20 cm. The SF-M is crosslinked in 75% ethanol for 30 minutes. Using ethanol as the dispersing liquid, a nanoscale fiber suspension is prepared under the conditions of a power of 270W and ultrasonic fragmentation with an ice bath for 30 minutes. The ethanol is removed by centrifuging at 7000 rpm for 15 minutes. The SF short fibers are then frozen at −80°C for at least 12 hours, followed by freeze-drying for 12 to 18 hours to obtain silk fibroin lyophilized staple fibers (SF-S).

Preparation of Biomimetic Sponge Dressing

A collagen solution at a concentration of 0.55 mg/mL is mixed individually or in combination with 20 μg/mL of Fn and 10 mg/mL of rLys to form a composite collagen solution. This collagen gel is then used to coat the silk fibroin staple fibers and shaped with an appropriate cell mold. After being frozen overnight at −80°C, it undergoes freeze-drying to obtain four types of Col/SF-S-based dressings: Col/SF-S, Fn-Col/SF-S, rLys-Col/SF-S, and Fn-rLys-Col/SF-S. The liquid volume and freeze-drying duration are different depending on the cell culture plate specifications. The sample volumes for 96-well, 48-well, and 6-well plates were 100 μL, 0.8 mL, and 2 mL, respectively, with freeze-drying durations of 8 hours, 10 hours, and 16 hours.

Physicochemical Characterization

Morphological Analysis

Scanning Electron Microscopy (SEM) was used to characterize the morphological changes during the preparation of the dressing. The SF, SF-S, and Fn-rLys-Col/SF-S samples were gold-sputtered and imaged at an acceleration voltage of 15 kV. Random sampling of SF-S and Fn-rLys-Col/SF-S materials was conducted using ImageJ software, and the diameters and apertures of 100 fibers were measured.

Evaluation of Water Absorption and Retention

The samples were divided into Col/SF-M, Col/SF-S, Fn-rLys-Col/SF-S, and SHISHOU groups. After being dried in a vacuum oven for 12 hours, the samples were weighed, and the initial mass was recorded as M_1. After swelling in PBS to equilibrium, the samples were weighed as M_2. The weight at intervals of 10 min, 30 min, 2 h, 4 h, 6 h, 8 h, 12 h, and 24 h was recorded as M_3. The water absorption rate was calculated by Eq.1.

$$\text{Water absorption rate}\,(\%) = \frac{\text{M3} - \text{M1}}{\text{M1}} \times 100\% \tag{1}$$

The samples were then placed at room temperature, and their weights were recorded at intervals of 2, 4, 6, 8, 10, 12, and 24 hours as M_4. The water retention rate was calculated by Eq.2.

$$\text{Water retention rate}\,(\%) = \frac{\text{M2} - \text{M4}}{\text{M2} - \text{M1}} \times 100\% \tag{2}$$

Evaluation of Sustained Release and Degradation Rate

The four types of Col/SF-S-based dressings were immersed in PBS, and 20 μL of the release liquid was extracted at 37°C at intervals of 2, 3, 4, 5, 12, and 24 hours and measured for its A562 value using the BCA method. The initial mass of the four types of Col/SF-S-based dressings was recorded as M_1. They were immersed in PBS and retrieved at 37°C on days 1, 3, 5, 7, 14, and 21, then freeze-dried and weighed as M_2. The degradation rate was calculated using the following Eq.3.

$$\text{Degradation rate}\,(\%) = \frac{\text{M1} - \text{M2}}{\text{M1}} \times 100\% \tag{3}$$

The evaluations of water absorption, retention, sustained release, and degradation rates for all samples were repeated three times.

Adhesion Test

Phosphate-buffered saline was used to wash tissue samples from multiple organs such as the heart, liver, spleen, kidneys, and muscles of mice. The prepared Fn-rLys-Col/SF-S were separately adhered to tissue wound surfaces with residual blood. After 5 seconds, the tissue interfaces were immediately separated and photographed for documentation.

Antibacterial Testing of Dressings in vitro

Bacterial Barrier Performance Under Semi-Humid Conditions

10 μL of bacterial solutions with a concentration of 10^8 CFU/mL of *S. aureus, E. coli*, and *P. aeruginosa* were dripped onto the center and corners of Col/SF-M, Col/SF-S, and SHISHOU. After incubating at 37°C for 24 hours, photographs were taken to record the plaque conditions.

Antibacterial Testing

0.2 mL of bacterial solutions with a concentration of 1×10^5 CFU/mL of methicillin-sensitive and MRSA were separately inoculated onto 0.6 g of four types of Col/SF-S-based dressings and a penicillin-loaded dressing group (PG-Col/SF-S), with a blank medium serving as the control group. At 37°C, 100 μL of bacterial solution was taken at 0, 2, 3, 4, 5, and 12 hours to measure OD values, and the inhibition rate was calculated using Eq.4.

$$\text{Inhibition rate}\,(\%) = \frac{\text{OD Group\_control} - \text{OD Group\_sub}}{\text{OD Group\_control}} \times 100\% \tag{4}$$

Biocompatibility and Biofunction of Dressings in vitro

Hemocompatibility Assay

Col/SF-M, Col/SF-S, Fn-rLys-Col/SF-S, and SHISHOU dressings were immersed in 0.9% saline, with 0.9% saline as the negative control and pure water as the positive control. Each group was treated with 0.2 mL of sheep whole blood in a 37°C water bath for 1 hour, followed by centrifugation at 1000 $r{\cdot}min^{-1}$ for 5 minutes. The absorbance (A) of the supernatant at 545 nm was measured, and the hemolysis rate was calculated using Eq.5.

$$\text{Hemolysis rate}\,(\%) = \frac{\text{A Group\_sub} - \text{A Group\_NC}}{\text{A Group PC} - \text{A Group\_NC}} \times 100\% \quad (5)$$

Coagulation Performance Assay

100 μL of sheep whole blood and 10 μL of 0.2 $mol{\cdot}L^{-1}$ calcium chloride solution were dripped onto the surface of Col/SF-M, Col/SF-S, Fn-rLys-Col/SF-S, and SHISHOU dressings. After incubating in a 37°C water bath for 5 minutes, 10 mL of pure water was added to remove uncoagulated blood. The solution was collected, and its OD value at 540 nm was measured. Anticoagulated blood without added materials served as the blank control, and the coagulation rate was calculated using Eq.6.

$$\text{Coagulation rate (BCI)}\,(\%) = \frac{\text{A Group\_sub}}{\text{A Group\_NC}} \times 100\% \quad (6)$$

Cell Culture

Fifth-passage human foreskin fibroblast (HFF) cells were used to evaluate the biocompatibility of the dressings. The cells were cultured in DMEM medium containing 10% fetal bovine serum at 37°C and 5% CO_2, with medium changes every two days, and logarithmic growth phase cells were used.

Live Cell Staining and Cytocompatibility

The CCK-F method was used to assess cell viability after co-culturing with the dressings. HFF cells at a density of 1×10^4 were seeded in 24-well plates containing Col/SF-M and Col/SF-S based dressings for co-culture. At 1, 7, and 11 days, 100 μL of Calcein-AM working solution was added per well under 37°C and 5% CO_2 conditions. After a 20-minute incubation in the dark, samples were imaged using a fluorescence microscope to assess cell growth within the dressings. The CCK-8 assay was used to evaluate the effect of the dressings on cell proliferation. HFF cell suspensions at 1×10^4 cells/mL were seeded in 96-well plates containing different scaffold groups, and CCK-8 reagent was added at 1, 3, 5, 7, and 9 days. After a 3-hour incubation, 100 μL of the supernatant was measured for OD at 450 nm using a microplate reader. Each experiment was repeated three times for accuracy.

Cell Migration Assay

To assess cell migratory ability, HFF cells were cultured in 6-well plates at a density of 5×10^5 cells per well. Once 90% confluent, a 1 mm diameter parallel wound was created on the monolayer using a 200 μL disposable pipette tip. Cells were then exposed to media containing various dressing samples. Cell migration was monitored and photographed at 0, 8, and 12 hours after treatment. Wound areas that remained unhealed (A_0 as the initial wound area, A_t as the wound area at each measurement time point) were analyzed using Photoshop 2019, and cell migration rate was calculated using Eq.7.

$$\text{Migration rate}\,(\%) = \frac{\text{A0} - \text{At}}{\text{A0}} \times 100\% \quad (7)$$

Experiments in vivo

All in vivo experiments were conducted in accordance with the National Institutes of Health (NIH) Guide for the Care and Use of Laboratory Animals, and were approved by the Animal Ethics Committee of Hangzhou Medical College, Hangzhou, China (No. 2023-049).

Wound Healing in vivo

Each New Zealand rabbit was housed individually in a cage, and the temperature in the animal room was maintained at 25°C with a relative humidity of 50% to ensure a clean environment with continuous access to food and water. The New Zealand rabbits used in the study, each weighing approximately 2 kg, were sourced from the Experimental Animal Center of Hangzhou Medical College. Anesthesia was induced via an auricular vein injection of urethane, and the rabbits were fixed in a prone position. The surgical area was shaved and disinfected, and a skin punch was used to create circular full-thickness skin defects of 2 cm diameter on the rabbit's back. A total of 60 defects were created and divided into five groups, each covered with Col/

SF-M, Col/SF-S, Fn-rLys-Col/SF-S, and SHISHOU dressings, with alternate-day dressing changes and untreated (blank control). Wound photographs were taken on days 0, 3, 9, 14, and 21 post-surgery and healing rates were calculated using Photoshop 2019 software for computer graphics processing and the following formula (8)

$$\text{Wound healing rate}\,(\%) = \frac{\text{Initial wound area} - \text{Unhealed wound area}}{\text{Initial wound area}} \times 100\% \tag{8}$$

Antibacterial Assay in vivo

On day 3, sterile swabs were used under sterile conditions to collect bacteria from the wound and the surrounding 0.5 mm area and placed in 50 mL of 0.9% sterile saline. After shaking for half an hour, 10 μL of the solution was spread on LB agar plates and incubated at 37°C for 12 hours to form observable colony units.

Histological Observation

On days 14 and 21 post-treatment, newly formed tissues from the wound sites of each group of New Zealand rabbits (six rabbits at each time point) were collected under anesthesia, fixed, dehydrated, trimmed, embedded, sectioned, and subjected to hematoxylin-eosin (HE) staining, Masson's trichrome staining, and immunohistochemistry (IHC) staining for IL-6 and VEGFA. The slides were then mounted and observed using a digital slide scanner for image capture. Initially, tissue images were captured at 40× magnification to examine general pathological changes, followed by images of specific lesion areas at 100× magnification. The ImageJ image analysis system was used to quantitatively evaluate epidermal thickness and collagen volume fraction. Specifically, the average epithelial thickness at the wound site was defined as α_1, and that of adjacent normal skin as α_2. The epidermal thickness index was calculated using formula (9):

$$\text{Epidermal thickness index} = \frac{\alpha 1}{\alpha 2} \times 100\% \tag{9}$$

Quantitative Real-Time PCR

Quantitative real-time PCR (qRT-PCR) was used to detect expression levels of different molecules in wounds treated by each group. Target genes included interleukin-6, interleukin-10, vascular endothelial factor VEGFA, CD34, and transforming growth factors TGF-β_1 and TGF-β_3. Total RNA from wound tissues was extracted using TRIzol Reagent, and cDNA synthesis was performed using the Evo M-MLVRT Mix Kit. Finally, SYBR Green Pro Taq HS Premix (2×) was used for qRT-PCR, with GADPH as the reference gene. Primer sequences for the target and reference genes are shown in Table 1.

Statistical Analysis

Statistical analysis of experimental data was performed using GraphPad Prism 9.0 (Graph-Pad Software, CA, USA). One-way analysis of variance (ANOVA) was used, followed by Bonferroni post hoc tests to determine statistical significance. Measurement data are presented as mean ± standard deviation (SD), and differences between groups were analyzed using variance analysis. Levels of statistical significance are represented as follows: $P<0.05$, $P<0.01$, $P<0.001$, $^{**}P<0.0001$.

Table 1 Summary of Primers for Target Genes and Reference Genes in qRT-PCR

	Forward Sequence	Reverse Sequence
IL-6	ATGAACTCCTTCACAAGCGCC	GAAGTGGGGAAAGCGGTAGC
IL-10	CGATTTCTCCCCTGTGAAAACAA	AGATGTCAAACTCACTCATGGCT
VEGFA	AAGGAGACAATAAACCCCACGAA	ACGCAGGAAGGCTTGAATATGTA
CD34	CAGAACTTTCCAGCATGTTCCAG	CAATCAAGGTCTTCCGGGAGTAG
TGF-β_1	TCTGGAACGGGCTCAACATC	AGTTCTTCTCTGTGGAGCTGAAG
TGF-β_3	CCAATTACTGCTTCCGCAAC	TAGTAGCCCTTGGGTTCGTG
GADPH	TCACCATCTTCCAGGAGCGA	TTTTGGCTCCGCCCTTCAAA

Results

Physicochemical Characterization

Silk fibroin membranes (SF-M) are obtained through electrospinning, as shown in Figure 1A. SEM images reveal that SF-M consists of randomly interconnected nanofibers with uniform diameters and porosity. SF-M was ultrasonically fragmented to obtain silk fibroin short fibers (SF-S), which appeared as powder after freeze-drying, with stacked short fibers visible under a scanning electron microscope (Figure 1B). A collagen composite solution loaded with lysozyme and fibronectin (Fn) was mixed with SF-S, and after freeze-drying, yielded the fibronectin-lysozyme-collagen/silk fibroin short fiber (Fn-rLys-Col/SF-S) biomimetic dressing. The Fn-rLys-Col/SF-S dressing exhibited a porous, sponge-like appearance (Figure 1C), with a large cellular honeycomb structure under electron microscopy. The pore walls formed a cord-like structure due to the presence of the staple fibers. During the early stages of wound healing and regeneration, the biomimetic dressing should provide mechanical support to cells and newly formed ECM while establishing an interconnected pore network to facilitate cell infiltration, angiogenesis, and nutrient diffusion.[29] The unique cord-like micro-nano structure of Fn-rLys-Col/SF-S enhances cellular adhesion and promotes directional cell growth, supporting the physical performance requirements of its biomimetic ECM. As shown in Figure 1D and E, compared to SF, the fiber diameter of SF-S significantly decreased after ethanol crosslinking treatment, and the stability of the short fiber morphology was significantly improved. The results in Figure 1F indicate that the introduction of collagen and other components caused moderate fiber swelling, with the final fiber diameter being (1.80±0.12) μm, and the diameter distribution became more concentrated. As shown in Figure 1G and H, compared to the SF nanomembrane, Fn-rLys-Col/SF-S exhibited a more orderly aperture structure, with an average aperture of (25.27±2.50) μm, and the uniformity of aperture distribution was significantly improved. This phenomenon can be attributed to the optimization of the preparation process, where a gradient cooling combined with freeze-drying technique was used on electrospun fibers. By controlling the ice crystal growth process, uniform, round ice crystals were formed, and after freeze-drying, a three-dimensional scaffold with regular pore structures was obtained. This composite preparation process effectively overcame the limitations of single electrospinning technology, such as uneven aperture distribution and its adverse effects on cell growth.

Maintaining moisture balance in the wound bed plays a crucial role in wound closure. The moist wound healing theory requires dressings to possess both high fluid absorption and long-lasting moisturizing capabilities.[30] To this end, this study systematically evaluated the water absorption and retention rates of the materials, using commercially available dressings as controls. As shown in Figure 1I, Col/SF-S and Fn-rLys-Col/SF-S reached water absorption saturation within 10 minutes, with water absorption rates exceeding 2000% of their own mass, significantly higher than Col/SF-M and the commercial dressings ($P < 0.0001$). This phenomenon confirms that the three-dimensional sponge-like porous structure formed by short fibers through freeze-drying exhibits a stronger fluid absorption capacity than the two-dimensional structure of Col/SF-M and the coarse fiber macroporous structure of commercial products. This difference is attributed to the high specific surface area and capillary effect of the three-dimensional structure, resulting in significantly better fluid absorption efficiency compared to the loose fiber network of commercial products. The rapid fluid absorption characteristic of the materials can promptly remove excess exudate, preventing maceration damage to the surrounding skin, while the delayed absorption of commercial products may weaken this protective effect. Notably, there was no statistically significant difference in water absorption performance between Col/SF-S and Fn-rLys-Col/SF-S, confirming that the loading of Fn and rLys did not affect the fluid absorption characteristics of the materials.

The assessment of water retention performance showed (Figure 1J) that the water retention rates of all samples decreased in a time-dependent manner. Col/SF-S and Fn-rLys-Col/SF-S exhibited rapid water loss in the first 2 hours, followed by a sustained-release phase from 2–12 hours, and complete water loss after 12–24 hours. This two-stage release pattern can maintain a more lasting moist microenvironment for the wound bed, which is beneficial for cell migration. In contrast, the rapid evaporation rate of moisture due to the large pore size of commercial dressings may lead to premature drying of the wound bed, increasing the risk of delayed healing and scar formation.

The release timing of active substances Fn and rLys from the biomimetic Fn-rLys-Col/SF-S dressing is a crucial factor in regulating wound healing. Figure 1K shows an initial burst release at 2 hours due to the rapid dissolution of surface-free proteins on Col/SF-S, Fn-Col/SF-S, rLys-Col/SF-S, and Fn-rLys-Col/SF-S. From 2 to 5 hours, the drug

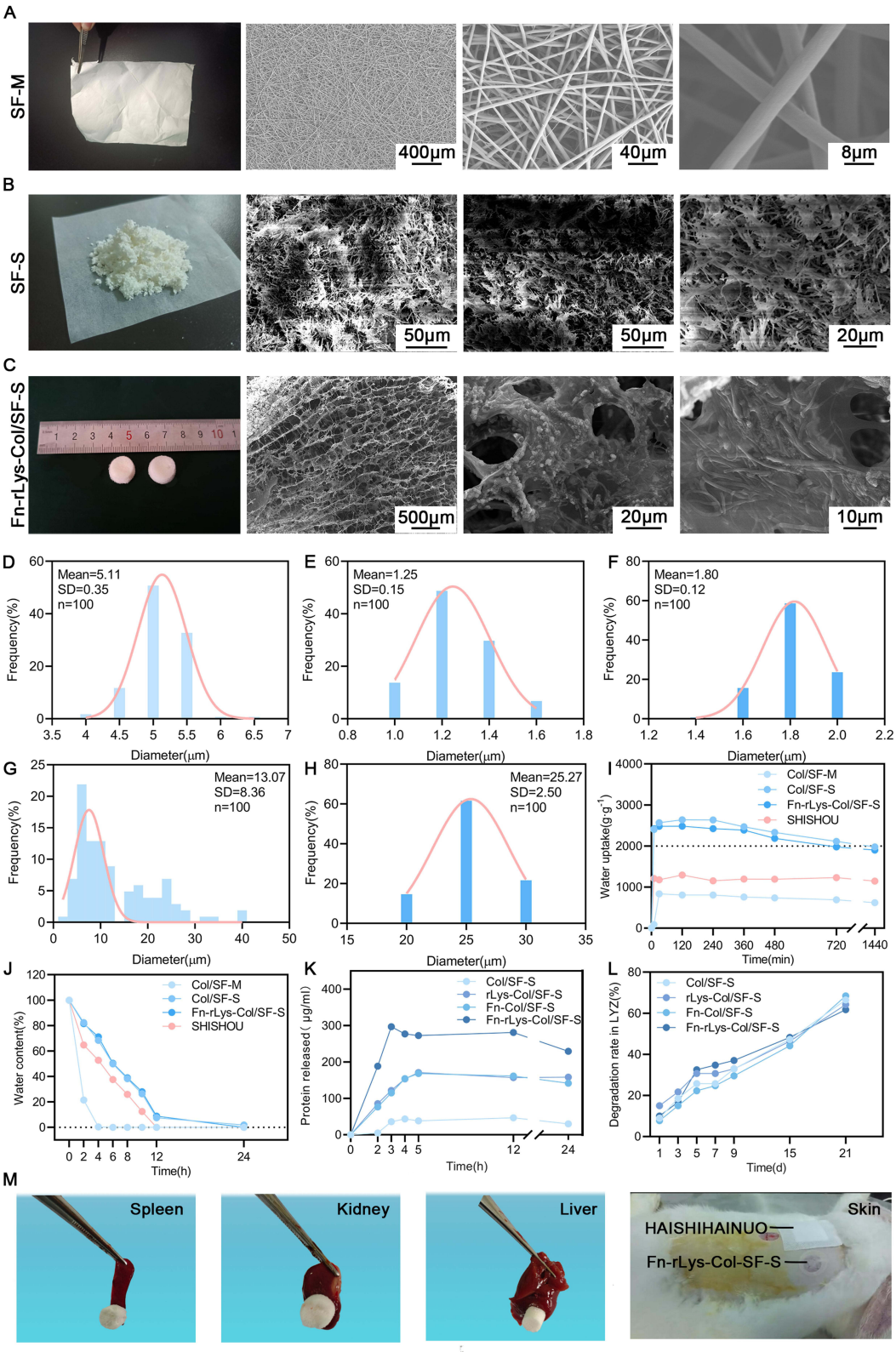

Figure 1 Physical characterization of the dressings.

Notes: (**A**–**C**) Macroscopic views and scanning electron microscopy images of SF-M, SF-S, and Fn-rLys-Col/SF-S. (**D**–**F**) Fiber diameters of SF-M, SF-S, and Fn-rLys-Col/SF-S. (**G** and **H**) Pore sizes of SF-M, SF-S, and Fn-rLys-Col/SF-S. (**I** and **J**) Water absorption and retention of the dressing were measured by the gravimetric method. (**K**) The BCA method detected the protein release rate of the dressing within 24 hours in a neutral environment. (**L**) Degradation rate of the dressing in lysozyme over 21 days (37°C, pH=7.4). (**M**) Images of apparent adhesion properties of Fn-rLys-Col/SF-S to different organ tissues.

release curve stabilized due to the dressing's three-dimensional and uniform porous structure. From 5 to 48 hours, protein release reached a stable state, suggesting that Col/SF-S and Fn-rLys-Col/SF-S provide slow protein release, allowing continuous regulation of the wound. Further in vitro degradation experiments of these dressings (Figure 1L) showed that on day 21, the degradation rates of Col/SF-S, Fn-Col/SF-S, rLys-Col/SF-S, and Fn-rLys-Col/SF-S were 66.45%, 68.43%, 64.23%, and 61.76%, respectively, with no statistical difference, indicating that the Col/SF-S dressing base possesses degradability in vitro, reducing dressing change frequency and preventing secondary injury caused by adhesion in traditional cotton gauze dressings.[31] The degradability of the dressing is mainly attributed to the hydrophilic natural biomaterials used as raw materials, providing both degradability and biocompatibility.

Figure 1M shows that Fn-rLys-Col/SF-S exhibits excellent compliance, adhering well to the surface of soft tissues with different curvatures and textures (such as myocardium, liver, or wound tissue). Through capillary action, it absorbs moisture from the organ surface and conforms well to its shape, providing an optimized interface contact and mechanical microenvironment for wound healing. However, its tensile strength, elasticity, and other mechanical properties could not be measured, and further optimization of its mechanical properties is needed in the future.

Antibacterial Testing of Dressings in vitro

Bacterial infections often lead to persistent or excessive inflammatory responses and tissue necrosis in wounds, severely disrupting the healing process.[32] Among infected wounds, *S. aureus, E. coli*, and *P.aeruginosa* are the most common pathogens.[33] Among them, MRSA infections are the most serious due to the improper use of antibiotics.[34] Therefore, this study primarily evaluates the bacterial barrier performance against the most clinically prevalent wound infection pathogens - *S. aureus, E. coli*, and *P.aeruginosa*, with antibacterial assessment specifically conducted on *S. aureus* and MRSA. Among the various methods of preparing antibacterial dressings, we employ a dual antibacterial strategy: constructing a three-dimensional nanoscale fibrous network to physically block bacteria and loading the dressing with lysozyme to ensure wounds are protected from pathogens. Specifically, we tested Col/SF-M, Col/SF-S, and commercial products for their adherence blocking effects against the three most common wound pathogens (*S. aureus, E. coli*, and *P. aeruginosa*), with commercial products serving as the control group. Additionally, we compared the bactericidal effect of biosynthetic lysozyme with penicillin against *S. aureus* and MRSA.

Figure 2A shows that Col/SF-S exhibited no significant bacterial plaques and had the best blocking effect against the three strains, whereas commercial products and Col/SF-M were less effective, displaying visible bacterial plaque overflow. This is because the diameter of short fibers is similar to that of the bacteria, making them prone to bacterial adhesion,[35] and the three-dimensional structure of Col/SF-S can further block cocci penetration. Furthermore, each group had a better blocking effect on *S. aureus* than on *P.aeruginosa* and *E. coli*, as *S. aureus* is spherical, has a diameter of 0.8 μm, and lacks flagella, resulting in a larger size and less mobility, making it easier to be blocked.[36] Agar plate experiment results (Figure 2B and C) show that the dressing loaded with rLys effectively killed *S. aureus* and MRSA, especially demonstrating superior antibacterial properties against MRSA compared to penicillin. To examine the release of antibacterial properties from the rLys-loaded dressing, it was co-cultured with *S. aureus* and MRSA. After 12 hours, the culture medium of the rLys-loaded dressing remained clear, indicating minimal bacterial growth, while the solution of the blank group and the PG-loaded MRSA solution turned turbid, indicating significant bacterial growth (Figure 2D and E). Further optical density (OD) value detection of bacterial solutions (Figure 2F and G) indicates that compared to dressings containing PG, the dressings with rLys possess good bactericidal properties, achieving an inhibition rate of over 70% against *S. aureus* and drug-resistant bacteria within 12 hours ($P<0.0001$). Between 5 and 12 hours, the antibacterial effect of penicillin gradually weakened, while the antibacterial effect of lysozyme continually strengthened, suggesting that this advantage is due to the bactericidal mechanism of lysozyme and the sustained-release property of the dressing. Therefore, the lysozyme-loaded nanofiber dressing possesses a dual antibacterial effect, structurally inhibiting and compositionally killing bacteria, which may offer a solution for clinically susceptible drug-resistant *S. aureus*. Future studies will systematically evaluate the inhibitory effects of the dressing on fungi (such as *Candida albicans*) and anaerobic bacteria (such as *Bacteroides fragilis*) to more comprehensively assess its clinical application potential.

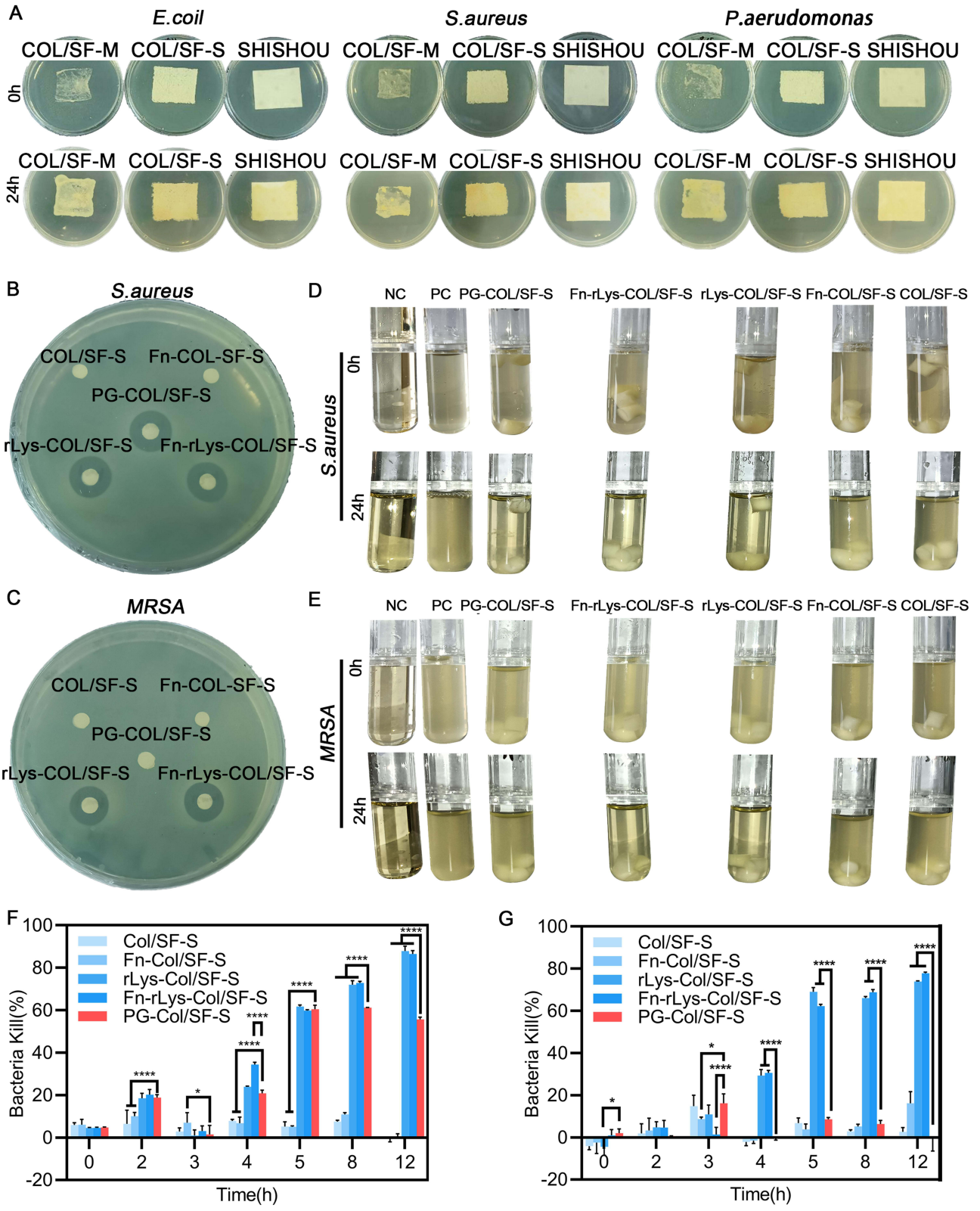

Figure 2 Antibacterial performance of the dressings in vitro.

Notes: (**A**) The antibacterial effectiveness of Col/SF-M, Col/SF-S, and SHISHOU against *Staphylococcus aureus*, *Escherichia coli*, and *P. aeruginosa* under semi-wet conditions. (**B** and **C**) Co-culture of Staphylococcus aureus (**B**) and MRSA (**C**) with Col/SF-S, Fn-Col/SF-S, PG-Col/SF-S, rLys-Col/SF-S, and Fn-rLys-Col/SF-S on agar plates, where the size of the inhibition zone is proportional to the antibacterial performance. (**D** and **E**) Images of the blank group, rLys-Col/SF-S, Fn-rLys-Col/SF-S, PG-Col/SF-S, Fn-Col/SF-S, and Col/SF-S after being exposed to Staphylococcus aureus (**D**) and MRSA (**E**) cultures for 24 hours. (**G** and **F**) Antibacterial rates against Staphylococcus aureus (**G**) and MRSA (**F**) were assessed by measuring the OD values of the bacterial cultures in the blank group, rLys-Col/SF-S, Fn-rLys-Col/SF-S, PG-Col/SF-S, Fn-Col/SF-S, and Col/SF-S groups. Data are presented as mean ± SD (n=3), *P < 0.05, ****P < 0.0001.

Biocompatibility and Biofunction of Dressings in vitro

For contact medical dressings, excellent hemocompatibility is essential and is determined by hemolysis testing.[37] Figure 3A and B show that when blood was exposed to Col/SF-M, Col/SF-S, and Fn-rLys-Col/SF-S dressings, their hemolysis rates were (4.45±0.19)%, (4.63±0.73)%, and (4.93±0.11)%, respectively, all below 5% and meeting industry standards.[38] Notably, the hemolysis rates were significantly reduced compared to the commercial product group ($P<0.0001$), supporting the non-irritating and safe direct application of naturally sourced materials for wound healing.[39] During the hemostatic phase of wound healing, uncontrolled bleeding is a major cause of death from traumatic events. Hemostatic dressings can help stop bleeding and promote wound closure.[40] The hemostatic performance of dressings is evaluated by calculating the blood clotting index (BCI), where a lower BCI indicates better hemostatic performance. In vitro BCI results showed that, compared to commercial products, the BCI of Col/SF-M, Col/SF-S, and Fn-rLys-Col/SF-S was significantly decreased ($P<0.0001$), and clearly coagulated blood clots were observed on their surfaces, indicating good hemostatic properties of the experimental dressings. In contrast, the blood components in the commercial product group dispersed in deionized water, indicating poor hemostatic effect (Figure 3C and D). These results suggest that the biomimetic dressing has good biocompatibility and provides effective hemostatic capability due to the presence of collagen. Extensive studies have also confirmed that collagen[41,42] and silk fibroin[43,44] can activate coagulation pathways through various mechanisms, promoting hemostasis.

Typically, three days after skin injury, wound repair enters the proliferation phase dominated by activities such as fibroblast proliferation, migration, and matrix secretion. The duration of the proliferation phase is crucial for wound healing.[45] Ideally, dressings should have good biocompatibility, function as cell scaffolds, and actively induce cell proliferation and migration.[46] When co-cultured with experimental dressings using HFF as a model, live cell fluorescence staining microscopic images (Figure 3E) showed that the density of green fluorescent cells in dressing groups increased over time, with the Fn-containing dressing group displaying higher cell viability on day 11, nearly fully covered by green live cells. In contrast, fluorescence in the blank group diminished after 7 days, with reduced live cell numbers, cell rounding, and gradual disintegration. CCK-8 assay results for cytotoxicity in dressing groups (Figure 3F) indicated that HFF co-cultured with dressings displayed a continuous proliferation trend for 11 days without significant cytotoxicity. The Fn-containing dressing showed no statistical difference in proliferation trends from the blank group within days 1–5, exceeding other experimental groups, while proliferation persisted in the dressing group from days 7–11, significantly higher than the blank and nanomembrane groups ($P>0.0001$). The blank group's cells began disintegrating and undergoing apoptosis due to contact inhibition. Experimental results confirmed that the three-dimensional structure of the dressing group is conducive to continual cell growth and reproduction. The OD value of proliferating cells in the Fn-containing dressing group remained higher than that of other dressing groups within 11 days, indicating that Fn promotes fibroblast proliferation, consistent with previous studies.[47,48]

Studies have shown that enhancing cell migratory capacity can promote wound healing. In the text, a scratch test was used to evaluate the inducibility of cell migration in the HFF cells by the dressing group. The experimental results showed that within 16 hours (Figure 3G and H), the wound healing rate in the Col/SF-S group was above 70%, and compared to the blank group, the cell migration rate increased significantly ($p\leq0.05$). Among them, the dressing group loaded with Fn had the highest cell migration rate (90%), indicating that the dressing containing Fn has effective bioactivity and functionality to promote wound healing, which is related to the fact that Fn can significantly enhance the migratory capacity of fibroblasts.[49]

Experiments in vivo

An in vivo wound healing experiment was conducted using a full-thickness skin defect model on the back of New Zealand white rabbits to evaluate the effectiveness of Fn-rLys-Col/SF-S in treating deep wounds. As shown in Figure 4A, circular full-thickness skin defects with a diameter of approximately 10mm were created on both sides of the rabbit's back. The experimental group was covered with the dressing, while untreated blank and commercially treated groups served as controls. Figure 4B and C show that the wound area in each group gradually decreased over time. The commercially available product group, blank group, and fiber membrane group had dry wounds with thicker scabs, whereas the short fiber group had moist wounds without dressing adhesion. The wound healing rates for Col/SF-S (59.8 ± 2.47) % and Fn-rLys-Col/SF-S (63.3 ± 2.82)

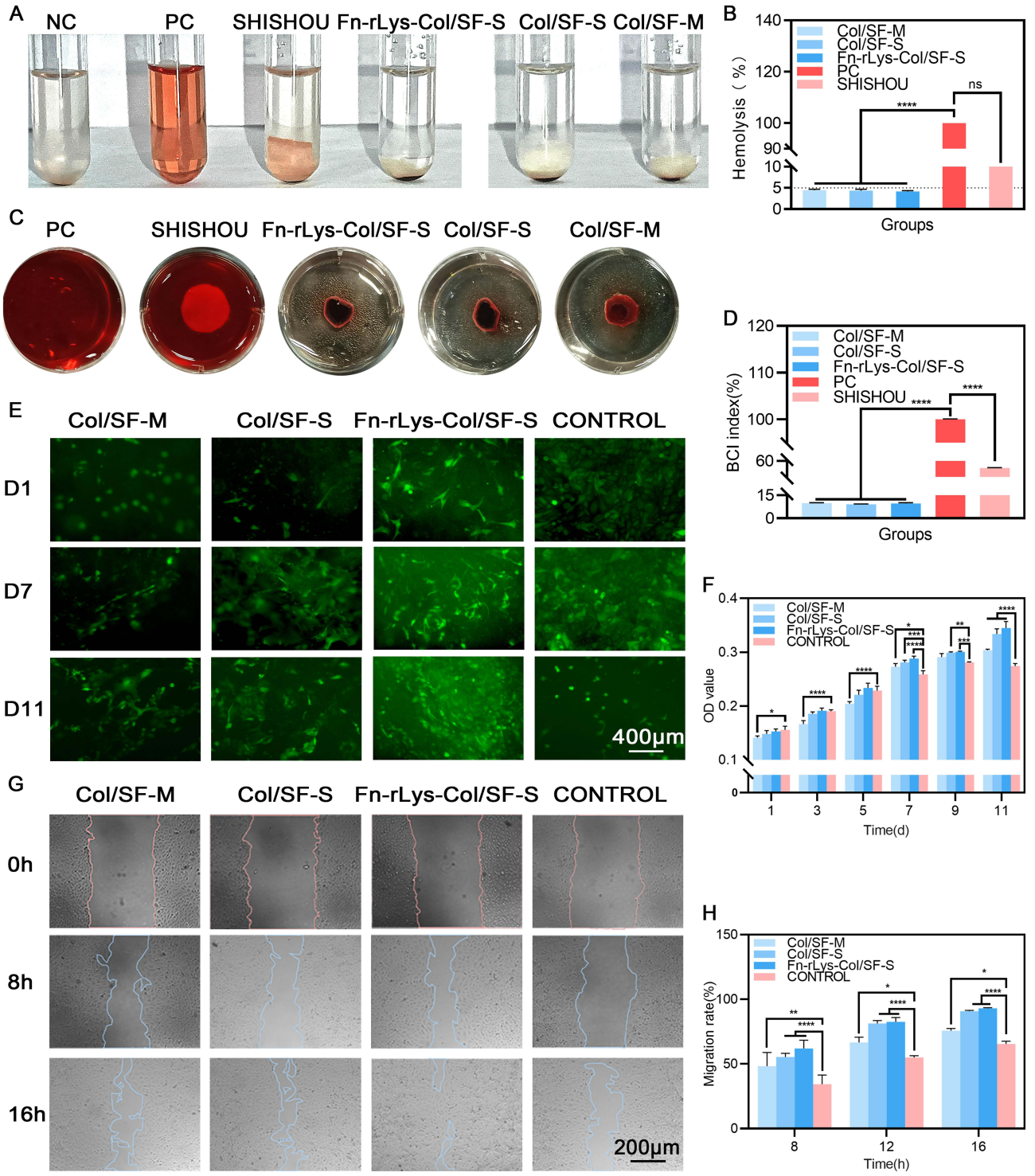

Figure 3 Evaluation of dressing blood reactivity and biocompatibility.

Notes: (**A** and **B**) Hemolysis images (**A**) and statistical analysis of hemolysis rate (**B**). (**C** and **D**) Coagulation experiments and the statistical analysis of coagulation indices. (**E**) Fluorescence staining images of live HFF cells after incubation with the dressings. (**F**) Assessment of cytotoxicity of each dressing group using the CCK-8 method. (**G** and **H**) Physical images of HFF migration and changes at different time points, along with a statistical quantitative analysis of migration capability. Data are presented as mean ± SD(n=3), *P < 0.05, ** P < 0.01, ***P < 0.001, ****P < 0.0001.

Abbreviation: ns, not significant.

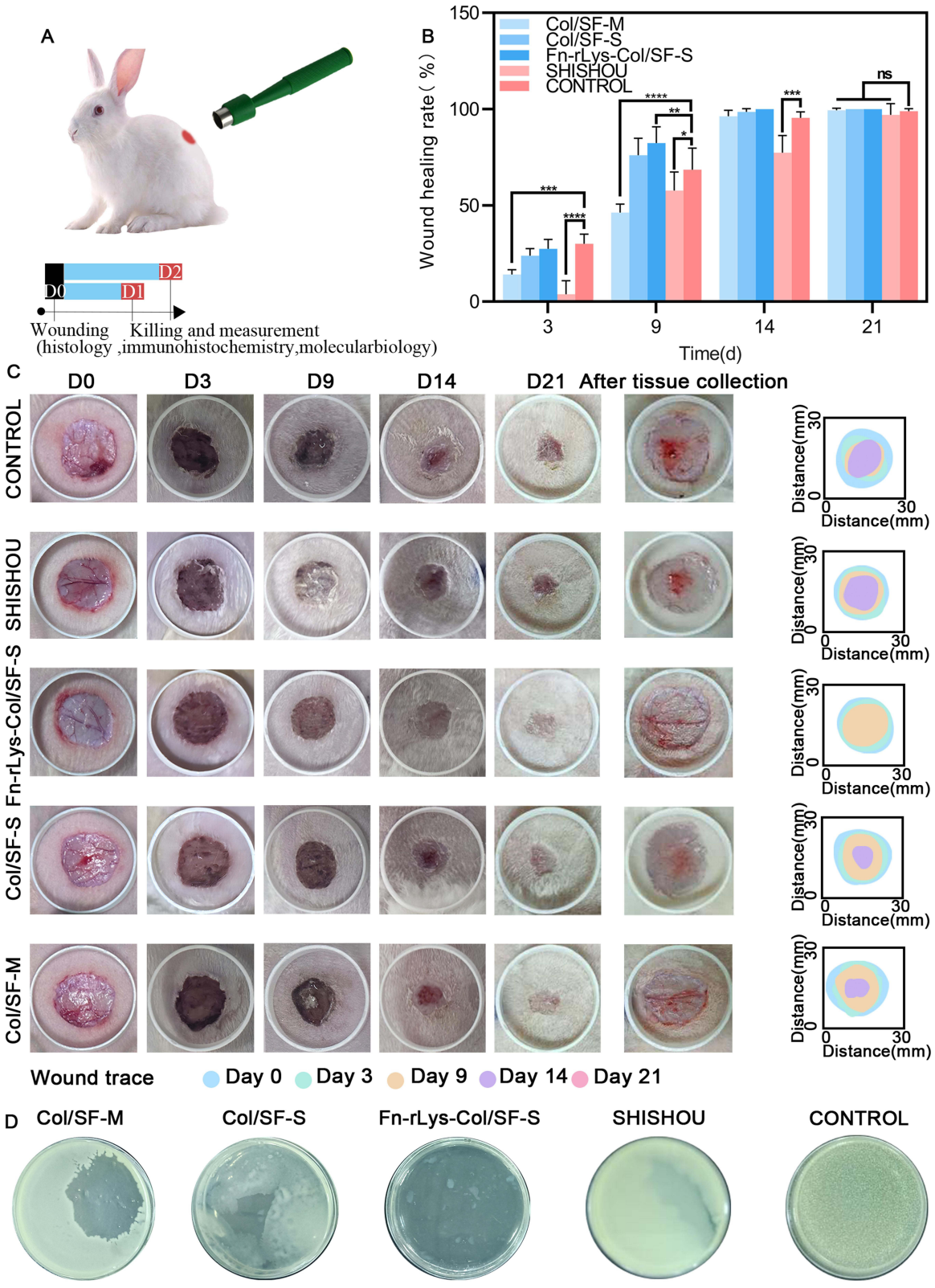

Figure 4 Effects of dressings on skin defect healing in vivo.

Notes: (**A**) Schematic of full-thickness wound model in New Zealand rabbits. (**B**) Wound healing rates of each dressing group on days 3, 9, 14, and 21. (**C**) Overlay images of wound traces at different time points (days 0, 3, 9, 14, 21) after tissue collection. (**D**) Representative images of viable bacterial colonies collected from wounds. Data are presented as mean ± SD(n=3), *P < 0.05, ** P < 0.01, ***P < 0.001, ****P < 0.0001.

Abbreviation: ns, not significant.

https://doi.org/10.2147/IJN.S521956

% were significantly higher than those of the control and commercial groups. The control group achieved wound closure at 21 days, while the Fn-rLys-Col/SF-S group completed closure in 14 days, shortening the healing process by 7 days. At day 21, new hairs had grown over the newly formed skin in this group, and further sampling revealed no adhesion between the new skin's subcutaneous and fascial layers, with the skin structure intact. Other groups exhibited adhesive bleeding.

Bacterial sampling and culture detection from the wound surface in each group showed (Figure 4D) that the Fn-rLys-Col/SF-S group had the lowest bacterial load, while the commercially available product group had the highest, indicating that rLys exerted antibacterial bioactivity.

H&E staining and Masson staining were used to evaluate the therapeutic efficacy of each material group in the wound healing process from a histopathological perspective. The H&E staining results are shown in Figure 5A. On the 14th day post-surgery, the Fn-rLys-Col/SF-S treatment group showed a complete skin stratification structure on the wound, with clear identification of the stratum corneum, stratum germinativum, and dermis. The remaining groups still exhibited stratum corneum defects and eschar residue. On the 21st day, the Fn-rLys-Col/SF-S and Col/SF-S groups showed thinned and flattened epidermis in the wound, most closely resembling normal skin tissue structure. The epidermis of the remaining groups was significantly uneven and thickened, with tongue-like projections at the edges, similar to keloids. Further analysis of epidermal thickness (Figure 5B) and epidermal thickness index (Figure 5C) of each group revealed that on the 21st day, the epidermal thickness of the Fn-rLys-Col/SF-S and Col/SF-S groups were (35.64±1.08) μm and (33.16±0.26) μm, respectively. The epidermal thickness of normal skin cells was (35.14±1.23) μm. Compared to the other groups, the epidermal thickness index was closest to 1 ($p<0.0001$).

Collagen is the main component of the ECM and is crucial for wound repair.[50] Masson staining of the wound tissue sections is shown in Figure 5D. After modeling, the remaining groups did not show the formation of obvious skin appendages such as blood vessels, hair follicles, and sebaceous glands in the wound. However, the Fn-rLys-Col/SF-S group began to form blood vessels. At 21 days, the Fn-rLys-Col/SF-S and Col/SF-S groups had formed mature granulation tissue, including hair follicles and blood vessels, and the collagen deposition formed an orderly basket-weave arrangement, exhibiting normal dermal characteristics. Furthermore, at 21 days, the amount and arrangement of collagen produced by Fn-rLys-Col/SF-S treatment were closest to normal skin (Figure 5E), with a collagen deposition rate of (72±0.01) %, demonstrating the best dermal collagen remodeling.

FN has been proven to promote angiogenesis. To verify whether Fn-rLys-Col/SF-S can release rLys and FN to inhibit inflammation and promote angiogenesis, VEGFA and IL-6 immunohistochemical tests were performed on the neotissue at 14d and 21d. The immunohistochemical staining results of VEGFA in tissue sections are shown in Figure 5F. On the 14th day of treatment, the number of VEGFA-positive cells in each group was higher than that in the blank control group. On the 21st day, the number of VEGFA-positive cells in each experimental group decreased to varying degrees, and the number of VEGFA-positive cells in the Fn-rLys-Col/SF-S group was (47.33±0.58) cells/HPF (Figure 5G), which was significantly higher than that in the blank control group ($P<0.0001$). The results indicate that Fn-rLys-Col/SF-S can effectively promote the expression of VEGFA in the early stage of wound healing, reaching the peak earliest, and maintaining a high level of expression later, which can effectively promote neovascularization. Figure 5H shows the IL-6 staining results. On the 14th day, the CONTROL group, SHISHOU and COL/SF-M group had strong inflammatory reactions, and the number of brown-yellow cells was visibly and widely distributed. The Fn-rLys-Col/SF-S and Col/SF-S groups had milder inflammatory reactions, and the number of positive cells was (16.33±0.58) cells/HPF and (21.00±1.00) cells/HPF, respectively (Figure 5I). At 21 days, the inflammatory response of each group decreased, and the number of IL-6 positive cells in the Fn-rLys-Col/SF-S group was (6.66±1.15) cells/HPF, significantly lower than that of the CONTROL group ($P<0.0001$), confirming that it effectively controls the inflammatory cascade through antibacterial effects.

Through histological experiments, we discovered that Fn-rLys-Col/SF-S, leveraging its nanoscale three-dimensional structure and the bioactive properties of loaded Fn or rLys, synergistically promotes wound healing by reducing inflammation, accelerating angiogenesis, and promoting collagen deposition. To further investigate the pro-healing mechanism of Fn-rLys-Col/SF-S, we performed RT-qPCR to detect the effect of different material treatments on the expression levels of IL-6, IL-10, CD34, VEGFA, TGF-β_1, and TGF-β_3 related genes in the newly formed skin of each group. Figure 6A–F show that the mRNA of active factors in all experimental groups exhibited an overall trend of increasing first and then decreasing. At 21 days, the expression of active factors in the wounds of the Fn-rLys-Col/SF-S

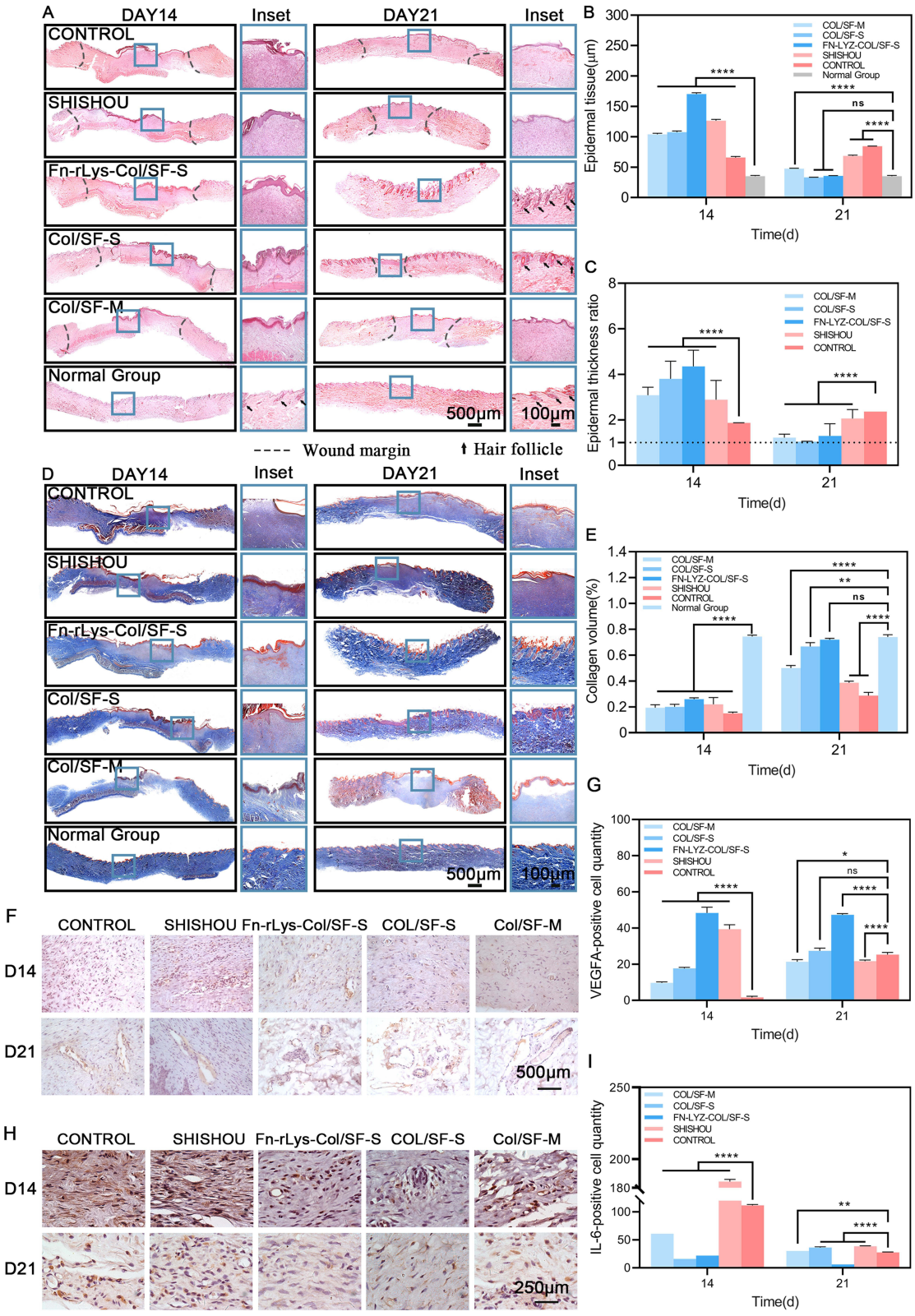

Figure 5 Analysis of the effects of dressings on full-thickness wound healing in rabbits.
Notes: (**A**) HE staining images of regenerated tissue on days 14 and 21. (Figure caption: Black arrows indicate hair follicles.) (**B** and **C**) Epithelial tissue thickness and Epithelial ratio thickness of skin tissues after various treatments through HE staining. (**D**) Masson staining of newly formed skin on days 14 and 21. (**E**) Collagen volume fraction of skin tissues after various treatments through Masson staining. (**F** and **G**) Immunohistochemical staining of VEGFA and quantification of VEGFA-positive cells in wound areas. (**H** and **I**) Immunohistochemical staining of VEGFA and quantification of VEGFA-positive cells in wound areas. Data are presented as mean ± SD(n=3), *P < 0.05, ** P < 0.01, ****P < 0.0001.
Abbreviation: ns, not significant.

https://doi.org/10.2147/IJN.S521956

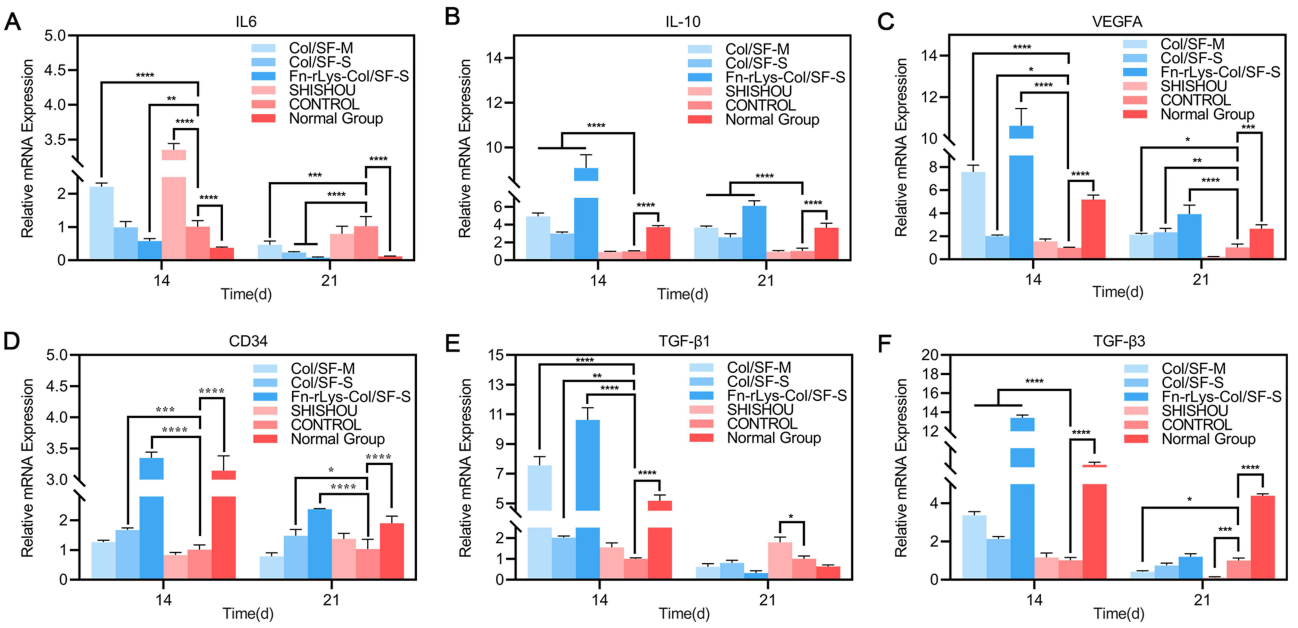

Figure 6 Relative mRNA expression levels.

Notes: (**A–F**) Relative expression levels of mRNA for genes such as IL-6, IL-10, VEGFA, CD34, TGF-β_1, and TGF-β_3 in wounds, detected by qRT-PCR. Data are presented as mean ± SD(n=3), *P < 0.05, ** P < 0.01, ***P < 0.001, ****P < 0.0001.

treatment group was closest to the factor expression of normal skin, indicating that the microenvironment of the new skin also tended to be normal skin. During the wound healing process, compared with the blank control group, Fn-rLys-Col /SF-S can down-regulate the expression of the pro-inflammatory factor IL-6 and the scar growth factor TGF-β_1, while up-regulate the expression of the anti-inflammatory factor IL-10, the pro-angiogenic factors VEGFA and CD34, and the transforming growth factor TGF-β_3, thereby reducing the inflammatory response, accelerating angiogenesis, and regulating and limiting scar formation. This result is consistent with the aforementioned histological results.

Discussion

The primary internal challenge of skin defect regeneration lies in the lack of a medium for dermal cell migration and attachment, as well as an appropriate microenvironment for cell proliferation. As a result, cells are unable to crawl and regenerate tissue to cover the wound. Additionally, the external environment poses threats such as bacterial infections, making it difficult for wounds to close.[51] To address these issues, various biomimetic nanofiber membranes have been widely applied in skin tissue regeneration. Furthermore, to enhance the speed and efficacy of skin tissue regeneration, a variety of functional factors are extensively utilized, including growth factors, chemokines, antimicrobials, microRNAs,[52] and oxygen. For example, Zhang et al improved conventional gel-based wound dressings by incorporating freeze-dried oxygen-encapsulated nanoparticles. These nanoparticles delivered dissolved oxygen to the wound surface, and experimental results showed that they effectively promoted diabetic wound healing.[53]

Current two-dimensional nanofiber membranes prepared using electrospinning technology possess high porosity, but the small pore size formed by fiber stacking significantly limits cell infiltration, growth, and the delivery efficiency of macromolecular nutrients. To overcome these limitations, this study employed ultrasonic fragmentation technology to process nanofiber membranes into short fibers, which were then combined with a collagen loaded with rLys and Fn. Using freeze-drying technology, porous sponge-like Fn-rLys-Col/SF-S biomimetic dressings were fabricated. The resulting material exhibited a large pore size structure of (25.27±2.50) μm, with pore walls composed of nanoscale short fibers with a diameter of (1.8±0.12) μm. This structure highly mimics the topological and biochemical properties of natural ECM, providing an optimal microenvironment for fibroblasts adhesion, migration, and proliferation. Its high specific surface area and porosity confer superior water-vapor exchange and protein slow-release performance, while simultaneously forming an effective physical barrier against bacteria.In terms of functional biomimetic design, the Fn

loaded in the dressing activates the integrin-FAK signaling pathway,[54] significantly enhancing cell proliferation, migration, and angiogenesis. Meanwhile, rLys specifically cleaves the pentaglycine bridges in the peptidoglycan of *S. aureus*,[55] and experimental results have demonstrated its significant bactericidal effect against MRSA, providing an effective strategy to address clinical antibiotic resistance issues.

Notably, the dressing achieves the synergistic controlled release of Fn and rLys through pH-responsive collagen degradation. The decrease in local pH caused by inflammatory exudates at the wound site accelerates collagen degradation, promoting the rapid release of active ingredients. This mechanism not only effectively regulates the dynamic balance of inflammatory factors (reducing pro-inflammatory factor IL-6 and increasing anti-inflammatory factor IL-10) and scar-related factors (TGF-β_1 /TGF-β_3), but also significantly improves wound healing quality. This "structure-function" dual biomimetic design strategy provides an innovative research paradigm and technical pathway for the development of next-generation smart wound dressings.

Conclusion

In summary, this study innovatively developed a three-dimensional biomimetic Fn-rLys-Col/SF-S wound dressing by mimicking both the components (functional Fn and rLys) and three-dimensional topological structure (micro-nano fiber pore size and diameter) of the ECM, achieving integrated physical bacterial inhibition, chemical sterilization, and regeneration promotion. This dressing not only retains the ECM-simulating structural properties of electrospun nanofibers but also effectively addresses key limitations of traditional two-dimensional nanofilms (Col/SF-M), including small pore size and insufficient cell infiltration. Systematic in vitro experiments confirmed the Fn-rLys-Col/SF-S dressing's excellent comprehensive performance: outstanding liquid absorption capacity (absorbing over 20 times its own weight), significant antibacterial properties (77.8±0.31% bactericidal rate against MRSA, $p<0.0001$), and good hemostatic capability. Animal experiments further demonstrated that the dressing can significantly accelerate the healing process of full-thickness skin defects (reducing healing time by 33.33% compared to commercial products), promote regeneration of skin appendages (eg, hair follicles), and effectively inhibit scar formation. Based on its innovative structural design concept, clear therapeutic effects, and simple preparation process, the Fn-rLys-Col/SF-S dressing demonstrates significant clinical translational value. Moreover, its pH-responsive drug release characteristics provide broad prospects for its application as a multifunctional drug-delivery platform in biomedical fields such as tissue engineering and drug delivery.

In conclusion, Fn-rLys-Col/SF-S exhibits remarkable potential as a multifunctional wound dressing. Its superior biocompatibility and structural features not only facilitate wound regeneration, but also demonstrate translational prospects in tissue-engineering drug-delivery scaffolds. Through incorporation of varied bioactive components, this platform could enable personalized wound management strategies. Nevertheless, this study reveals two critical limitations requiring further investigation: 1) Systematic validation across diverse wound models using expanded animal cohorts and preclinical trials to establish therapeutic universality; 2) Development of standardized fabrication protocols to address challenges in process control and production scalability for industrial implementation. Addressing these issues would significantly advance the material's transition from experimental research to clinical translation.

Funding

The part of this research was funded by Scientific Research Fund of Zhejiang Provincial Education Department (Y202352014) and National Innovation and Entrepreneurship Training Program for College Students (202413023037X).

Disclosure

The authors report no conflicts of interest in this work.

References

1. Ye Y, Hong Y, Liang QM, et al. Bioinspired electrically stable, optically tunable thermal management electronic skin via interfacial self-assembly. *J Colloid Interface Sci*. 2024;660:608–616. doi:10.1016/j.jcis.2024.01.041
2. Choo JH, Kim D, Min K, Lee SY, Kang NG. Pogostemon cablin Extract Promotes Wound Healing through OR2AT4 Activation and Exhibits Anti-Inflammatory Activity. *Curr Issues Mol Biol*. 2024;46(8):9136–9148. doi:10.3390/cimb46080540
3. Khosrowpour Z, Bashiri Z, Jafari D, et al. Translation Prospects of a Novel ECM-Silk Fibroin/Alginate 3D-Printed Scaffold for Treatment of Full-Thickness Skin Wounds: an In Vitro and In Vivo Study. *Polym Adv Technol*. 2024;35(11):14.

4. Lin MOY, Sampath D, Bosykh DA, et al. YAP/TAZ Drive Agrin-Matrix Metalloproteinase 12-Mediated Diabetic Skin Wound Healing. *J Invest Dermatol*. 2025;145(1):18. doi:10.1016/j.jid.2024.07.011
5. Cai WN, Song Y, Xie Q, et al. Dual osmotic controlled release platform for antibiotics to overcome antimicrobial-resistant infections and promote wound healing. *J Control Release*. 2024;375:627–642. doi:10.1016/j.jconrel.2024.09.022
6. Zeng XL, Chen BH, Wang LP, et al. Chitosan@Puerarin hydrogel for accelerated wound healing in diabetic subjects by miR-29ab1 mediated inflammatory axis suppression. *Bioact Mater*. 2023;19:653–665. doi:10.1016/j.bioactmat.2022.04.032
7. Krauss S, Illg C, Held M, Daigeler A, Eisler W. A Quantitative Analysis of Microcirculation During Healing of Split-Thickness Skin Grafts in Standardized Full-Thickness Wounds. *Wounds-Compend Clin Res Pract*. 2024;36(5):177–182. doi:10.25270/wnds/23112
8. Mendes JF, Fontes MD, Barbosa TV, Paschoalin RT, Mattoso LHC. Membranes composed of poly(lactic acid)/poly(ethylene glycol) and Ora-pro-nobis (Pereskia aculeata Miller) extract for dressing applications. *Int J Biol Macromol*. 2024;268:15. doi:10.1016/j.ijbiomac.2024.131365
9. Alamre JB, Alkreathy H, Ali AS, Alfadil A, Alghamdi SS. Effect of 3-hydrazinylquinoxaline-2-thiol hydrogel on skin wound healing process in diabetic rats. *Sci Rep*. 2024;14(1):14. doi:10.1038/s41598-024-70849-x
10. Cheng S, Wang H, Pan X, et al. Dendritic Hydrogels with Robust Inherent Antibacterial Properties for Promoting Bacteria-Infected Wound Healing. *ACS Appl Mater Interfaces*. 2022;14(9):11144–11155. doi:10.1021/acsami.1c25014
11. Watson F, Chen R, Percival SL. In vitro prevention and inactivation of biofilms using controlled-release iodine foam dressings for wound healing. *Int Wound J*. 2024;21(1):10. doi:10.1111/iwj.14365
12. Qi X, Xiang Y, Li Y, et al. An ATP-activated spatiotemporally controlled hydrogel prodrug system for treating multidrug-resistant bacteria-infected pressure ulcers. *Bioact Mater*. 2025;45:301–321. doi:10.1016/j.bioactmat.2024.11.029
13. Cheng J, Wang RX, Hu YY, Li MX, You LJ, Wang SY. Fermentation-inspired macroporous and tough gelatin/sodium alginate hydrogel for accelerated infected wound healing. *Int J Biol Macromol*. 2024;268:13. doi:10.1016/j.ijbiomac.2024.131905
14. Qi X, Shi Y, Zhang C, et al. A Hybrid Hydrogel with Intrinsic Immunomodulatory Functionality for Treating Multidrug-Resistant Pseudomonas aeruginosa Infected Diabetic Foot Ulcers. *ACS Mater Lett*. 2024;6(7):2533–2547. doi:10.1021/acsmaterialslett.4c00392
15. Lv KN, Wang L, He XL, Li WJ, Han L, Qin S. Application of Tilapia Skin Acellular Dermal Matrix to Induce Acute Skin Wound Repair in Rats. *Front Bioeng Biotechnol*. 2022;9:10. doi:10.3389/fbioe.2021.792344
16. Wang ML, Yu DG, Bligh SWA. Progress in preparing electrospun Janus fibers and their applications. *Appl Mater Today*. 2023;31:15.
17. Yu X, Wu GB, Cai PF, et al. Carbon Fiber-Mediated Electrospinning Scaffolds Can Conduct Electricity for Repairing Defective Tendon. *ACS Appl Mater Interfaces*. 2024;16(39):52104–52115. doi:10.1021/acsami.4c12245
18. Naghashzargar E, Aghajani M, Ranjbar-Mohammadi M. The potential of an electrospun poly (3-hydroxybutyrate)/poly (ethylene glycol) blend fibrous scaffold for cartilage tissue engineering. *Int J Polym Mater Polym Biomat*. 2025;74(1):21–29. doi:10.1080/00914037.2024.2314598
19. Krysiak ZJ, Stachewicz U. Urea-Based Patches with Controlled Release for Potential Atopic Dermatitis Treatment. *Pharmaceutics*. 2022;14(7):10. doi:10.3390/pharmaceutics14071494
20. Lei L, Huang WH, Liu K, et al. Trilazad mesylate-loaded electrospun cellulose acetate nanofibrous wound dressings promote diabetic wound healing by modulation of immune response and protection against oxidative damage. *J Drug Deliv Sci Technol*. 2022;69:10.
21. Cestari M, Caldas BS, Fonseca DP, et al. Silk fibroin nanofibers containing chondroitin sulfate and silver sulfadiazine for wound healing treatment. *J Drug Deliv Sci Technol*. 2022;70:14.
22. Jy L, Yt L, Guo CL, Wu XC. Development of quercetin loaded silk fibroin/soybean protein isolate hydrogels for burn wound healing. *Chem Eng J*. 2024;481:12.
23. Arumugam M, Murugesan B, Chinnalagu DK, Mahalingam S. Dual therapeutic approach: biodegradable nanofiber scaffolds of silk fibroin and collagen combined with silver and gold nanoparticles for enhanced bacterial infections treatment and accelerated wound healing. *J Drug Deliv Sci Technol*. 2024;95:15.
24. Hemalatha T, Aarthy M, Sundarapandiyan A, Ayyadurai N. Bioengineered Silk Fibroin Hydrogel Reinforced with Collagen-Like Protein Chimeras for Improved Wound Healing. *Macromol Biosci*. 2024;2024:14.
25. Zha S, Utomo YKS, Yang L, Liang GZ, Liu WQ. Mechanic-Driven Biodegradable Polyglycolic Acid/Silk Fibroin Nanofibrous Scaffolds Containing Deferoxamine Accelerate Diabetic Wound Healing. *Pharmaceutics*. 2022;14(3):21. doi:10.3390/pharmaceutics14030601
26. Lake J, Zaniolo K, Gingras ME, Couture C, Salesse C, Guérin SL. Functional Impact of Collagens on the Activity Directed by the Promoter of the α5 Integrin Subunit Gene in Corneal Epithelial Cells. *Invest Ophthalmol Vis Sci*. 2015;56(11):6217–6232. doi:10.1167/iovs.15-16587
27. Zhao MP, Huang ML, Li Z. Exploring the therapeutic potential of recombinant human lysozyme: a review on wound management system with antibacterial. *Front Bioeng Biotechnol*. 2023;11:14. doi:10.3389/fbioe.2023.1292149
28. Le GN, Li YQ, Cai L, et al. Lysozyme-based nanozyme encapsulated in double-network hydrogel for monitoring and repair of *MRSA* infected wounds. *Chem Eng J*. 2023;477:17. doi:10.1016/j.cej.2023.146421
29. Lee YJ, Baek SE, Lee S, et al. Wound-healing effect of adipose stem cell-derived extracellular matrix sheet on full-thickness skin defect rat model: histological and immunohistochemical study. *Int Wound J*. 2019;16(1):286–296. doi:10.1111/iwj.13030
30. Xiao L, Ni WQ, Zhao XH, et al. A moisture balanced antibacterial dressing loaded with lysozyme possesses antibacterial activity and promotes wound healing. *Soft Matter*. 2021;17(11):3162–3173. doi:10.1039/D0SM02245D
31. Tang L, Guo ZY, Zhao Q, et al. A Biodegradable Janus Sponge for Negative Pressure Wound Therapy. *Biomacromolecules*. 2024;25(4):2542–2553. doi:10.1021/acs.biomac.4c00046
32. Yanagiuchi T, Kato T, Hirano K, et al. Predictors of delayed wound healing after simultaneous endovascular treatment and minor forefoot amputation for chronic limb-threatening ischemia with wound infection. *Vascular*. 2023;31(2):333–340. doi:10.1177/17085381211067601
33. Butsyk A, Varava Y, Moskalenko R, et al. Copper Nanoparticle Loaded Electrospun Patches for Infected Wound Treatment: from Development to In-Vivo Application. *Polymers*. 2024;16(19):18.
34. Dubey AK, Sharma M, Raut S, Gupta P, Khatri N, Khatri N. Healing wounds, defeating biofilms: lactiplantibacillus plantarum in tackling MRSA infections. *Front Microbiol*. 2023;14:13. doi:10.3389/fmicb.2023.1284195
35. Abrigo M, Kingshott P, McArthur SL. Electrospun Polystyrene Fiber Diameter Influencing Bacterial Attachment, Proliferation, and Growth. *ACS Appl Mater Interfaces*. 2015;7(14):7644–7652. doi:10.1021/acsami.5b00453
36. Zajmi A, Hashim NM, Noordin MI, et al. Ultrastructural Study on the Antibacterial Activity of Artonin E versus Streptomycin against Staphylococcus aureus Strains. *PLoS One*. 2015;10(6):12. doi:10.1371/journal.pone.0128157

37. Liu R, Xi P, Yang N, Luo Y, Cheng BW. Chitosan/poly (ethylene oxide) nanofiber sponge with dual-responsive drug release and excellent antibacterial property. *Int J Biol Macromol*. 2023;246:13.
38. Yang X, Chen M, Wang YZ, Si XQ, Hao JH, Shi CC. HNTs assembled sponge with enhanced mechanical properties and bioactivity for uncontrollable hemorrhage and wound healing. *Appl Mater Today*. 2024;37:13.
39. Xu HQ, Che YL, Zhou R, et al. Research progress of natural polysaccharide-based and natural protein-based hydrogels for bacteria-infected wound healing. *Chem Eng J*. 2024;496:20.
40. Liu Y, Zhang JX, Jin YZ, Yin ML. Gelatin methacrylate based liquid dressing with antibacterial and hemostasis properties. *Colloid Surf A-Physicochem Eng Asp*. 2024;689:8. doi:10.1016/j.colsurfa.2024.133749
41. Zhang XX, Cai L, Li GY. Bottom-up reconstitution design of a biomimetic atelocollagen microfibril for enhancing hemostatic, antibacterial, and biodegradable benefits. *J Mat Chem B*. 2024;2024:17.
42. Zhang XX, Yang CK, Zeng XL, Li GY. A bioactive composite sponge based on biomimetic collagen fibril and oxidized alginate for noncompressible hemorrhage and wound healing. *Carbohydr Polym*. 2024;343:17.
43. Li J, Wu HJ, He XD, et al. Silk fibroin aerogels with AIE-featured berberine and MXene for rapid hemostasis and efficient wound healing. *Int J Biol Macromol*. 2024;283:11.
44. Si RR, Wang YF, Yang YC, Javeed A, Chen JN, Han BN. Dynamic dual-crosslinking antibacterial hydrogel with enhanced bio-adhesion and self-healing activities for rapid hemostasis in vitro and in vivo. *Mater Des*. 2023;233:13. doi:10.1016/j.matdes.2023.112244
45. Yujra VQ, Silveira E, Ribeiro DA, Castilho RM, Squarize CH. Clock gene Per2 modulates epidermal tissue repair in vivo. *J Cell Biochem*. 2024;125(2):13. doi:10.1002/jcb.30513
46. Peltier S, Adib Y, Nicosia L, et al. In vitro effects of wound-dressings on key wound healing properties of dermal fibroblasts. *Exp Dermatol*. 2024;33(5):8.
47. Heras-Parets A, Ginebra MP, Manero JM, Guillem-Marti J. Guiding Fibroblast Activation Using an RGD-Mutated Heparin Binding II Fragment of Fibronectin for Gingival Titanium Integration. *Adv Healthc Mater*. 2023;12(21):10. doi:10.1002/adhm.202203307
48. Shukla A, Suresh V, Gupta PC, et al. A single chain variable fragment antibody (Tn 64) cognate to fibronectin type III repeats promotes corneal wound healing by inhibiting fibrosis. *Int Immunopharmacol*. 2024;133:11.
49. Erdogan B, Ao MF, White LM, et al. Cancer-associated fibroblasts promote directional cancer cell migration by aligning fibronectin. *J Cell Biol*. 2017;216(11):3799–3816. doi:10.1083/jcb.201704053
50. Dong YQ, Zhu WD, Lei XX, et al. Treatment of Acute Wounds With Recombinant Human-Like Collagen and Recombinant Human-Like Fibronectin in C57BL/6 Mice Individually or in Combination. *Front Bioeng Biotechnol*. 2022;10:14.
51. Fu W, Sun S, Cheng Y, et al. Opportunities and challenges of nanomaterials in wound healing: advances, mechanisms, and perspectives. *Chem Eng J*. 2024;495:153640. doi:10.1016/j.cej.2024.153640
52. Shi L, Song D, Meng C, Cheng Y, Wang B, Yang Z. Opportunities and challenges of engineered exosomes for diabetic wound healing. *Giant*. 2024;18:100251. doi:10.1016/j.giant.2024.100251
53. Yang Z, Chen H, Yang P, et al. Nano-oxygenated hydrogels for locally and permeably hypoxia relieving to heal chronic wounds. *Biomaterials*. 2022;282:121401. doi:10.1016/j.biomaterials.2022.121401
54. Digiacomo G, Tusa I, Bacci M, Cipolleschi MG, Dello Sbarba P, Rovida E. Fibronectin induces macrophage migration through a SFK-FAK/CSF-1R pathway. *Cell Adh Migr*. 2017;11(4):327–337. doi:10.1080/19336918.2016.1221566
55. Gonçalves BV, Portela R, Lobo R, et al. Role of MurT C-Terminal Domain in the Amidation of Staphylococcus aureus Peptidoglycan. *Antimicrob Agents Chemother*. 2019;63(10). doi:10.1128/AAC.00957-19.